Published in final edited form as:
Mol Cell. 2014 July 17; 55(2): 171–185. doi:10.1016/j.molcel.2014.05.009.

Regulatory interactions between RNA and Polycomb Repressive Complex 2

Catherine Cifuentes-Rojas[1,2,3], **Alfredo J. Hernandez**[4], **Kavitha Sarma**[1,2,3], and **Jeannie T. Lee**[1,2,3,*]

[1]Howard Hughes Medical Institute, Boston, MA 02114, USA

[2]Department of Molecular Biology, Massachusetts General Hospital, Boston, MA 02114, USA

[3]Department of Genetics, Harvard Medical School, Boston, MA 02115, USA

[4]Department of Biological Chemistry and Molecular Pharmacology, Harvard Medical School, Boston, MA 02115, USA

SUMMARY

Polycomb repressive complex 2 (PRC2) is a histone methyltransferase that is localized to thousands of mammalian genes. Though important to human disease and as a drug target, how PRC2 is recruited remains unclear. One model invokes *cis*-regulatory RNA. Herein, we biochemically and functionally probe PRC2's recognition of RNA using the X-inactivation model. We observe surprisingly high discriminatory capabilities. While SUZ12 and JARID2 subunits can bind RNA, EZH2 has highest affinity and is somewhat promiscuous. EED regulates the affinity of EZH2 for RNA, lending greater specificity to PRC2-RNA interactions. Intriguingly, while RNA is crucial for targeting, RNA inhibits EZH2's catalytic activity. JARID2 weakens PRC2's binding to RNA and relieves catalytic inhibition. We propose that RNA guides PRC2 to its target, but inhibits its enzymatic activity until PRC2 associates with JARID2 on chromatin. Our study provides a molecular view of regulatory interactions between RNA and PRC2 at the chromatin interface.

INTRODUCTION

Polycomb repressive complex 2 (PRC2) are highly conserved factors first identified for body plan regulation in the fruitfly, *Drosophila melanogaster* (Muller and Verrijzer, 2009;Simon and Kingston, 2013). The catalytic subunit, EZH2, catalyzes the trimethylation of histone H3 at lysine 27 [H3K27me3] (Muller and Verrijzer, 2009;Margueron and Reinberg, 2011;Simon and Kingston, 2013) and establishes a chromatin structure that is repressive to transcription (Yuan et al., 2012). In mammals, PRC2 also plays crucial roles

*Correspondence to: lee@molbio.mgh.harvard.edu.

during development and disease pathogenesis (Schuettengruber and Cavalli, 2009;Margueron and Reinberg, 2011;Helin and Dhanak, 2013). For example, PRC2 subunits are frequently overexpressed or mutated in cancer, EZH2 overexpression is a poor prognosis for some cancers (Schuettengruber and Cavalli, 2009;Margueron and Reinberg, 2011;Helin and Dhanak, 2013), and disrupting EZH2 interactions can suppress cancer growth (Qi et al., 2012;Kim et al., 2013). Because of their clinical significance, PRC2 subunits have become high-priority drug targets (Helin and Dhanak, 2013). Still missing, however, is critical information regarding how PRC2 is targeted to specific loci and how it alters gene expression. Indeed, PRC2 binds locus-specifically to thousands of sites without an obvious sequence-specific DNA-binding subunit.

Several targeting mechanisms have been proposed. In the fruitfly, PRC2 interacts with sequence-specific binding proteins that recognize Polycomb response elements (PRE) (Ringrose and Paro, 2004;Schwartz and Pirrotta, 2008). In mammals, consensus motifs are not apparent, but PRC2 preferentially binds CpG-rich domains (Ku et al., 2008;Sing et al., 2009;Woo et al., 2010) and the DNA-binding factor, JARID2, may aid chromatin binding in some contexts (Lee et al., 2006;Peng et al., 2009;Shen et al., 2009;Li et al., 2010;Pasini et al., 2010). Long noncoding RNAs have emerged as potential guides, with *cis*-regulatory transcripts in particular being capable of tethering PRC2 to the site of transcription and directing its activity to the underlying chromatin. For instance, direct interactions between PRC2 and RepA/Xist RNAs target PRC2 *in cis* to the mammalian X-chromosome (Zhao et al., 2008). In the XCI model, PRC2 recruitment can be biologically separated from chromatin loading and catalytic activity of PRC2, with the antisense Tsix RNA being critical in this context (Zhao et al., 2008;Jeon and Lee, 2011). *Trans*-acting RNAs, such as HOTAIR (Rinn et al., 2007;Kaneko et al., 2010;Rinn and Chang, 2012), also interact with PRC2. PRC2 is now known to interact with a large portion of the mammalian transcriptome (Khalil et al., 2009;Kanhere et al., 2010;Zhao et al., 2010;Lee, 2012;Rinn and Chang, 2012;Mercer and Mattick, 2013), with one study indicating the capability of associating with >9,000 transcripts (Zhao et al., 2010). The large interactome has led two studies to conclude that PRC2 binds RNA promiscuously (Davidovich et al., 2013;Kaneko et al., 2013). It is possible, therefore, that RNA engages PRC2 for two distinct purposes — on the one hand, to recruit PRC2 locus-specifically (e.g., Xist/RepA (Zhao et al., 2008)) and, on the other, to interact more generally with PRC2 for as yet undetermined purposes on a genome-wide scale (Khalil et al., 2009;Kanhere et al., 2010;Zhao et al., 2010;Lee, 2012;Rinn and Chang, 2012;Davidovich et al., 2013;Kaneko et al., 2013;Mercer and Mattick, 2013).

Improved understanding of the role of RNA would aid pharmaceutical design and inform novel therapeutic strategies. While much of the current research is aimed at interfering with PRC2's methyltransferase activity, effective strategies may also target PRC2's interaction with RNA when there is evidence of regulatory action. Herein, using the XCI model, we parse PRC2's relationships to RNA, define regulatory interactions, and determine functional consequences. Our findings reveal a surprisingly large dynamic range of affinities for PRC2-RNA interactions, demonstrate specific regulatory roles for subunits, and identify RNA as a modulator of PRC2's methyltransferase activity.

RESULTS

PRC2 discriminates between cognate and nonspecific RNA

To investigate functional relationships via biochemical means, we purified assembled core subunits of mouse PRC2, various subcomplexes, and individual subunits by expressing FLAG-tagged constructs in baculovirus-infected insect cells. Core complexes were verified to contain EZH2, SUZ12, EED, and RBAP48 (Fig. 1A,B), to be catalytically active (Fig. 1C), and to be devoid of nucleic acids contaminants, as determined by spectrophotometry and 5′-end-labelling (data not shown). To evaluate PRC2-RNA binding, we first performed RNA electrophoretic mobility shift assays (EMSA) on known interacting RNAs, RepA (Zhao et al., 2008) and HOTAIR (Rinn et al., 2007). The 435-nt Repeat A domain of mouse RepA and Xist RNAs contains 8 units of a 28-nt repeat with the capacity to fold into double stem-loop structures (Fig. 1D) (Wutz et al., 2002;Maenner et al., 2010;Duszczyk et al., 2011;Minks et al., 2013). We observed that PRC2 robustly shifted RepA I-IV (Fig. 1E). A shorter 210-nt version of RepA containing only the proximal 4 repeats (RepA I-II) was similarly shifted by PRC2. Likewise, PRC2 shifted the first ~300 nt of human HOTAIR (mHotair 1-310, hHOTAIR 1-300) containing the domain shown to contact PRC2 (Kaneko et al., 2010;Tsai et al., 2010;Wu et al., 2013). While PRC2 could still bind a 200-nt version of hHOTAIR (hHOTAIR 1-200), binding to mHotair was abrogated when the RNA was truncated to 150 nt (mHotair 1-150)(Fig. 1E). We also examined binding to the reverse complement of RepA (antisense Tsix), previously shown to also interact with PRC2 (Zhao et al., 2008). EMSA indicated that PRC2 could shift Tsix I-IV (a probe of identical size to RepA I-IV), but only at higher concentrations of protein (Fig. 1F). Similarly, PRC2 shifted the truncated antisense versions, Tsix I-II and III-IV, only at higher concentrations.

On the other hand, PRC2 did not bind to RNAs of foreign species, including the first 300-nt of the mRNA encoding Maltose Binding Protein (MBP 1-300) of *Escherichia coli* and the 154-nt P4-P6 domain of the *Tetrahymena* ribozyme — foreign control RNAs that were not expected to have any specificity for PRC2 and which were also used in a previous study (Davidovich et al., 2013). No binding occurred even at 500-fold molar excess of PRC2 (1000 nM; Fig. 1E,F). In a competition assay, co-incubation of cognate RepA I-IV RNA and the non-ligand P4-P6 RNA revealed a large preference of PRC2 for RepA RNA (Fig. 1G, left panel). In fact, across all PRC2 concentrations, the fraction of RepA I-IV bound was virtually identical in the presence or absence of P4-P6, highlighting the huge preference of PRC2 for RepA I-IV over P4-P6. Co-incubation of HOTAIR with P4-P6 demonstrated a similar preference for HOTAIR over P4-P6 (Fig. 1G, right panel). We also challenged the PRC2-RepA interaction with unlabeled tRNA. While the RepA shift was competed out by unlabeled RepA I-IV at a 25-fold molar excess, tRNA could not compete, even at a 2,500-fold molar excess (Fig. 1H). To rule out an effect of the FLAG tag on RNA binding, we removed FLAG from the tagged EZH2 subunit using recombinant enterokinase and observed that PRC2 bound RepA similarly and continued to discriminate between RepA and MBP RNAs (Fig. S1). Additionally, a FLAG-GFP control protein did not shift RepA I-IV or MBP (Fig. S1). These data exclude an influence of the FLAG tag on PRC2-RNA interactions. Thus, in contrast to previous findings (Davidovich et al., 2013;Kaneko et al.,

2013), our data argue that PRC2 effectively discriminates between specific and nonspecific RNAs.

To quantify the discriminatory potential, we measured dissociation constants (K_d) using a double-filter binding assay, in which protein-bound RNAs are bound by a nitrocellulose filter and free RNAs are captured by an underlying nylon filter (Fig. 2A). To reach saturating levels, 11 RNA species (2 nM) were tested across three $\log_{10}$ concentrations of PRC2 (1–1,000 nM). Binding curves were fitted using a nonlinear regression model, with high R^2 values indicating excellent fit overall. The results revealed a large dynamic range (Fig. 2B). PRC2's affinity for the full RepA (I-IV) motif (K_d ~81 nM) and the 300-nt hHOTAIR (K_d ~93 nM) were highest, whereas affinities for MBP and P4-P6 were lowest. For nonspecific RNAs, binding curves were nearly flat (hence, $K_d \gg 1{,}000$ nM). In reciprocal experiments, we titrated RNA across 3 $\log_{10}$ concentrations (1–1,000 nM) against 50 nM PRC2 and observed similar K_d's (Fig. 2C and data not shown: 75 nM for RepA I-IV; 116 nM for hHOTAIR 1-300; 377 nM for mHotair 1-310; 1,650 nM for MBP 1-300). Collectively, these results demonstrate that PRC2 acutely discriminates between cognate and nonspecific RNA, irrespective of size, and that it is able to differentiate between them with an effective dynamic range of 10 to $\gg$ 1,000 nM.

Tsix RNA as regulator of RepA-PRC2 interactions

Binding to Tsix was of interest, given that the antisense counterpart of Xist/RepA was previously shown to antagonize loading of PRC2 onto *Xist* chromatin (Lee et al., 1999;Zhao et al., 2008). Because Tsix is expressed at >100 times higher levels than RepA (Zhao et al., 2008), Tsix could titrate PRC2 from RepA and thereby block initiation of XCI. Binding curves indicated that, while Tsix could clearly bind PRC2, the strength of interaction was 4- to 6-fold lower than for RepA I-IV (K_d ~321 nM for Tsix I-IV, ~454 nM for Tsix I-II; Fig. 2B). On the other hand, Tsix III-IV exhibited even lower affinity (K_d >1,000 nM). The intermediate affinity of Tsix I-IV in light of its vast molar excess *in vivo* suggested that Tsix could antagonize RepA-PRC2 interactions through mass action. *In vivo*, Tsix's overexpression blocks *Xist* induction and XCI (Wutz and Gribnau, 2007;Starmer and Magnuson, 2009;Wutz, 2011;Disteche, 2012;Lee, 2012). To test this idea, we performed competition experiments by titrating in cold Tsix competitors in increasing concentrations to determine effects on RepA-PRC2 interactions. Cold Tsix increasingly titrated away RepA-PRC2 binding between 10–1,000 fold molar excess over RepA (Fig. 2D). By contrast, nonspecific MBP RNA was only effective at 1,000-fold excess. Interestingly, the duplexed RepA:Tsix (I-IV) RNA was even less effective, suggesting that Tsix could be as effective a repressor of RepA-PRC2 interactions by directly titrating RepA RNA (through duplex formation). Evidence for the existence of RepA:Tsix duplexes was previously demonstrated *in vivo* (Ogawa et al., 2008). As a ligand for PRC2, however, duplex RNA appeared inert. Together, these data biochemically validate the potential of Tsix RNA to serve as competitive inhibitor of the RepA-PRC2 interaction through mass action.

EZH2 binds RNA with highest affinity and EED tempers the interaction

PRC2 is composed of four core subunits, SUZ12, EED, RBAP46/48, and EZH2. EED binds the H3K27me3 mark, and SUZ12 and EED are required for EZH2's catalytic activity (Cao

and Zhang, 2004;Cloos et al., 2008;Pasini et al., 2010;Margueron and Reinberg, 2011). The relationship of each subunit to RNA is currently unclear. To ask which subunit possesses RNA-binding capacity, we individually purified FLAG-tagged subunits and performed EMSA with each subunit. We found that only EZH2 and SUZ12 could bind RNA with high affinity. They displayed similar preferences for RepA and HOTAIR over truncated RepA and HOTAIR transcripts, P4-P6, and MBP (Fig. 3A,B; Fig. S2A,B). On the other hand, EED bound poorly to all tested RNAs (Fig. 3C; Fig. S2C), precluding the calculation of K_d's. Filter-binding assays demonstrated that EZH2 has extremely high binding affinities for cognate RNAs, with K_d's of ≈ 28–32 nM (Fig. 3D,F). Its affinity for RNA is greater than that of SUZ12 (K_d ≈ 86–235 nM) or assembled PRC2 (K_d ≈ 81–93 nM). In fact, EZH2 even bound nonspecific MBP with moderate affinity (Kd ≈ 380 nM), suggesting that EZH2 maybe somewhat "promiscuous" for RNA. Like PRC2, individual EZH2 and SUZ12 subunits showed lower affinity for mHOTAIR 1-150 (≈160 nM) and for non-specific RNAs (>300 nM) MBP, and P4-P6, with K_d's not being measurable in most cases (≫1,000 nM). K_d's of 20–30 nM are typical of high-affinity receptor-ligand interactions; K_d's of 100–500 nM are of moderate affinity; and those greater than 1,000 nM generally characterize low-affinity interactions. Our data therefore demonstrate that EZH2 binds RNA with high affinity, SUZ12 binds with moderate affinity, and EED does not bind to an appreciable extent.

Given the differences between EZH2 and whole PRC2, we asked if other subunits modulate EZH2-RNA interactions to impart specificity to RNA binding. We co-expressed relevant subunits of interest in Sf9 cells and purified the subcomplex via the FLAG tag. Analysis of subcomplexes showed that addition of EED to EZH2 (Fig. 3E; Fig. S2D) had a major effect on binding to cognate RNAs, increasing the K_d of EZH2 for RepA by 6-fold and for hHOTAIR by 12-fold (Fig. 3D–F; Fig. S2D). Addition of EED decreased even more the affinity of EZH2 for nonspecific RNAs. When EED was combined with SUZ12, SUZ12's affinity for cognate RNAs was changed modestly, potentially improving binding by ~2-fold, without changing affinity for nonspecific RNAs, which remained low. Interestingly, SUZ12 also moderated binding of EZH2 to RNA, as the EZH2-SUZ12 subcomplex exhibited a greater K_d for RepA than EZH2 alone (Fig. 3D–F; Fig. S2D). The addition of EED to the EZH2-SUZ12 subcomplex further increased the K_d for RepA I–IV by 2-fold. Altogether, these data indicate that EZH2 is a very high affinity RNA-binding protein — arguably somewhat promiscuous in its relationship to RNA — and that EED regulates EZH2's affinity for RNA to lend greater specificity to overall PRC2-RNA interactions.

RNA binding inhibits the methyltransferase activity of PRC2

Given EZH2/PRC2's strong interactions with RNA, we asked whether its histone methyltransferase activity (HMTase) is affected by RNA binding. We measured methylation rates on recombinant histones in a nucleosome array with or without RNA under conditions of saturating concentrations of S-adenosyl methionine (SAM) and nucleosomes (Qi et al., 2012), with PRC2 supplied at 150 nM -- slightly above K_d for RNA binding [Fig. 2]). Under these conditions, PRC2 catalyzed the transfer of the methyl group of S-adenosyl methionine (SAM) into H3 at a steady-state rate of 409 ± 12 nM min^{-1} (Fig. 4A,B,D). Intriguingly, when 150 nM PRC2 was pre-incubated with RepA I-IV, we observed an inhibition of

methyltransferase activity (Fig. 4A,B). This inhibition was dose-dependent, at 10 nM RepA, the methylation rate decreased 2-fold; at 100 nM, the rate decreased 5-fold; at 250 nM, there was nearly complete inhibition (Fig. 4C,D). The repressive effect was specific to the RNA and directly correlated with RNA binding affinities (Fig. 4C,D): RepA had highest affinity for PRC2 and showed greatest inhibition of methylation activity, with an IC_{50} of 9.7 nM; Tsix I-IV had intermediate affinity and showed moderate inhibition, with an IC_{50} of 47.9 nM; whereas MBP had poor affinity and showed weakest inhibition, with an IC_{50} of 981.8 nM (Fig. 4E). Furthermore, the double-stranded RepA:Tsix (I-IV) RNA was bound poorly by PRC2 (Fig. 2D) and demonstrated similarly poor inhibitory effects, with an IC_{50} of >1,000 nM. Differences in inhibitory effects were highly significant (Fig. 4F). Similar results were obtained when PRC2 was present below its K_d for RNA binding. For example, at 20 nM PRC2, we also observed that RepA, but not MBP, inhibited the HMTase activity in a dose-dependent manner, with IC_{50}'s similar to those obtained at 150 nM PRC2 (Fig. 4G).

We conclude that RNA inhibits the methyltransferase activity of PRC2 in a concentration-dependent manner, directly correlating with PRC2's RNA-binding affinity. Thus, while RepA RNA enhances locus-specific recruitment of PRC2 (Zhao et al., 2008), binding to RepA holds the catalytic activity of PRC2 in check, potentially separating PRC2 recruitment from the catalytic step. It is intriguing that RNA at very low concentrations (e.g., 0.1–10 nM) dampened PRC2's catalytic rate considerably, especially when PRC2 was in vast molar excess. We do not understand why, but several possibilities are worthy of consideration. First, each molecule of RepA could potentially bind multiple PRC2 complexes, as RepA consists of 8 repeat units. PRC2 may also exist inherently as multimers (Son et al., 2013). Alternatively, in the absence of additional cofactors (e.g., JARID2 – see below), HMTase inhibition may persist after RNA dissociates from PRC2.

JARID2 attenuates RNA binding and enhances EZH2 catalysis

The Jumonji and ARID-domain protein, JARID2, associates non-stoichiometrically with PRC2 and modulates PRC2's recruitment and enzymatic activity (Peng et al., 2009;Shen et al., 2009;Li et al., 2010). JARID2 was recently proposed to associate with ~100 transcripts in mouse embryonic stem (ES) cells and aid recruitment of PRC2 to chromatin (Kaneko et al., 2014). Furthermore, JARID2 serves as an intermediate between Xist RNA and PRC2 during XCI (da Rocha et al., 2014). To investigate how JARID2 interacts with RNA, we FLAG-tagged and purified JARID2 for RNA EMSA. JARID2 shifted RepA I-IV and the truncated RepA I-II, but shifted HOTAIR transcripts to a lesser extent (Fig. 5A). Binding curves showed that JARID2's affinity for RNA was an order of magnitude lower than EZH2's, with K_d's exceeding 250 nM even for the best ligand, RepA I-IV (Fig. 5B). Like core PRC2 subunits, JARID2 did not bind MBP or P4-P6. Therefore, while JARID2 does interact specifically with RNA, the strength of RNA binding is modest.

While having modest RNA affinity itself, JARID2 could modulate RNA binding within the context of core PRC2. When co-purified with EZH2 or SUZ12 individually, JARID2 did not affect RepA I-IV binding (Fig. 5C). Interestingly, when co-purified with whole PRC2, JARID2 significantly attenuated binding to RepA RNA (Fig. 5C, $P<0.001$). Similar attenuation was observed when JARID2 was co-purified with the EZH2:SUZ12:EED

subcomplex ($P<0.05$). JARID2's inhibitory effects were observed regardless of whether it was co-purified with PRC2 (Fig. 5C) or added to pre-assembled PRC2 (Fig. 5D). However, when added to EZH2 rather than co-purified, JARID2 exerted a modest but significant inhibitory effect on RNA binding (Fig. 5D). Notably, JARID2 could inhibit RNA-PRC2 interactions when present 5-fold below PRC2 concentrations (40 nM; Fig. 5D), congruent with JARID2's sub-stoichiometric interaction with PRC2 (Li et al., 2010). This effect was also observed at a concentration stoichiometric to PRC2 (Fig. 5D). To quantitate how JARID2 affects PRC2's affinity for RepA RNA, we performed reciprocal double filter-binding assays and obtained similar results regardless of whether we titrated in RNA (Fig. 5E) or a co-purified PRC2:JARID2 complex (Fig. S3). Whereas PRC2 alone exhibited a K_d of ~80 nM, the addition of JARID2 resulted in a nearly 3-fold increase in the K_d for RepA RNA, while having little influence on that for MBP RNA (Fig. 5E). When JARID2 was co-purified with PRC2 as a complex, the increase was >4-fold (Fig. S3). Collectively, these data demonstrate that JARID2 specifically decreases the affinity of PRC2 for RepA RNA. Thus, like EED, JARID2 modulates PRC2 binding to RNA.

Given that PRC2 activity is inhibited by RNA binding (Fig. 4) and that JARID2 attenuates PRC2's interaction with RNA (Fig. 5), we wondered whether JARID2 could enhance PRC2 action by loosening RNA's grip on PRC2. The addition of stoichiometric levels of JARID2 to PRC2 (150 nM as above) enhanced H3 methylation rates from 409 to 1318 nM min^{-1} (Fig. 6A;B left panel), consistent with previous findings (Li et al., 2010). On the other hand, addition of RepA RNA to PRC2 decreased methylation rates from 409 to 132 nM min^{-1} (blue trendlines, Fig. 6B left vs. right panels). Intriguingly, addition of JARID2 relieved PRC2 repression by RNA, boosting methylation rates from 132 to 496 nM/min (Fig. 6B right panel). Conversely, the addition of RepA retarded HMTase activity from 1318 to 496 nM/min (Fig. 6B middle panel). The JARID2's de-repressive effect was RNA-specific and dose-dependent (Fig. 6C,D), with differences being highly significant (Fig. 6E). The effect was greatest with the high-affinity RepA I-IV, intermediate with the lower-affinity Tsix RNA, and poor with the nonbinding MBP RNA. The inert RepA:Tsix I-IV duplex was also a poor inhibitor. Consistent with JARID2's de-repressive effect on PRC2's HMTase activity, the IC_{50} of RNA was increased in the presence of JARID2 (Fig. 6F vs 4E).

Similar results were obtained when the PRC2:JARID2 complex was supplied below the K_d for PRC2-RNA interactions. At 20 nM PRC2, stoichiometric addition of JARID2 increased the HMTase activity ~2-fold (Fig. 6G), consistent with results at 150 nM PRC2 (Fig. 6B, left panel). At 20 nM PRC2:JARID2, RepA, but not MBP, inhibited the HMTase activity in a dose-dependent manner, with IC_{50}'s comparable to those at 150 nM PRC2 (Fig. 6H). Taken together, these data show that, in the context of RNA-associated PRC2, JARID2 stimulates PRC2's methyltransferase activity by tempering the inhibitory effect of RNA. We therefore propose that JARID2's stimulation of PRC2 [as reported in the literature (Peng et al., 2009;Shen et al., 2009;Li et al., 2010;Kaneko et al., 2014)] may be due in part to its de-repressive effect — i.e., its inhibition of RNA's repressive effect on EZH2 catalysis.

DISCUSSION

Our study underscores the fact that RNA-PRC2 interactions cannot be viewed in binary terms (bound, unbound), as various subunits of PRC2 interact with RNA differently in both qualitative and quantitative terms. For example, EZH2 interacts with RNA with very high affinity (K_d ~20–30 nM), but binding results in catalytic inhibition. On the other hand, EED has low RNA binding potential ($K_d \gg 1000$ nM), but PRC2 complexes containing EED exhibit greater specificity for RNA. Furthermore, JARID2 has modest RNA binding potential, but its binding to PRC2 relieves EZH2's catalytic inhibition by loosening the association between the RNA inhibitor and EZH2. Thus, we believe that whole PRC2 is not generally promiscuous in its interactions with RNA. Interestingly, however, the EZH2 subunit may be more so. EZH2's high affinity for RNA may provide one explanation for the differences between what we observe here and that reported previously (Davidovich et al., 2013), if the amount of active EZH2 varies in different protein preparations. Alternatively, mouse and human PRC2 may have different properties *in vitro*. Attempts are currently underway to resolve the biochemical differences (C. Davidovich, C. Cifuentes-Rojas, T. Cech, and J.T. Lee, unpublished observations).

Our detailed biochemical analysis provides a first glimpse of molecular events between RNA and PRC2 at the chromatin interface, informing how PRC2's methyltransferase activity might be targeted and regulated. Our findings offer mechanistic explanations for previously published *in vivo* observations (Fig. 7A) and develop a multi-step model for the recruitment, loading, and enzymatic activation of PRC2 during XCI (Fig. 7B). As shown previously *in vivo* (Zhao et al., 2008), PRC2 is recruited locus-specifically by the *cis*-acting RepA/Xist RNA. Recruitment, however, is clearly separable from the steps of loading onto a chromatin nucleation site (Jeon and Lee, 2011) and H3K27 methylation *in vivo* (Zhao et al., 2008), as RIP (RNA immunoprecipitation) detects interactions between RepA/Xist RNA and PRC2 at a pre-XCI stage when PRC2 components and the H3K27me3 epitope do not pull down *Xist* chromatin by ChIP (chromatin immunoprecipitation). *In vivo*, expression of Tsix RNA inhibits loading of PRC2 onto chromatin (Zhao et al., 2008). Our present *in vitro* data suggest that Tsix titrates away RepA-PRC2 interactions (Zhao et al., 2008), either by sequestering PRC2 through mass action or by associating with Xist to form a duplex (Ogawa et al., 2008) that is inert to PRC2 binding (Fig. 2B,D). *In vivo*, RepA is present at <5 copies, whereas Tsix is present at 100–1,000 copies per chromosome and developmental downregulation of Tsix leads to loading of RepA-PRC2 onto chromatin (Zhao et al., 2008). While binding to RepA/Xist enables locus- and/or chromosome-specific recruitment of PRC2, it is intriguing that the bound RNA inhibits the methyltransferase activity of PRC2 (Fig. 4), perhaps holding the enzymatic activity in check until PRC2 is correctly loaded onto chromatin. We suggest that engagement of JARID2 (on chromatin) attenuates the strong attraction between EZH2 and RNA, relieving the enzymatic repression by RNA to initiate a cycle of H3K27me3 on chromatin.

Collectively, our findings enable biochemical separation of PRC2 action on the Xi: Locus-specific recruitment by RNA, chromatin loading of the whole complex, and trimethylation of H3K27. Our model has the potential to reconcile various paradoxical findings, particularly with respect to JARID2's relationship PRC2 and RNA. For example, JARID2

has been proposed to stimulate PRC2's interaction with RNA (da Rocha et al., 2014;Kaneko et al., 2014). This "stimulatory" relationship could be explained by the double-negative relationship defined by our biochemical analysis — by serving as an inhibitor of an inhibitor (RNA), JARID2 relieves the repressive effect of RNA on PRC2 catalysis, and therefore appears to be a stimulator of PRC2 activities on chromatin. JARID2 has also been proposed to either enhance or repress PRC2 recruitment to chromatin (Peng et al., 2009;Shen et al., 2009;Li et al., 2010). Our biochemical model implies that whether the relationship is positive or negative could depend on how JARID2 and PRC2 engage RNA.

While molecular details herein are viewed from the XCI perspective, they may apply to other PRC2-repressed loci with *cis*-regulatory RNA. Many such loci have now been identified, including a number of important disease-associated genes (Pandey et al., 2008;Khalil et al., 2009;Kanhere et al., 2010;Yap et al., 2010;Zhao et al., 2010;Nagano and Fraser, 2011). Our study has potential implications for drug design against PRC2. For instance, drugs may be directed not only against the catalytic domain of EZH2, but also at various subunits, including JARID2, and their regulatory interactions with RNA. In this way, therapeutic intervention could be targeted at site-specific recruitment, chromatin loading, and/or catalysis — biochemically separable steps at which interference could achieve a precise locus-specific response.

EXPERIMENTAL PROCEDURES

Protein Expression and Purification

Mouse PRC2 subunits were expressed in Sf9 insect cells using the bac-to-bac system (Invitrogen) as previously described (Kaneko et al., 2014). pFastBac1 expression vectors as well as baculovirus P2 stocks containing N-terminal FLAG-epitope tagged EZH2, SUZ12, and EED, as well as untagged SUZ12, EED, RBPA48 and JARID2 were obtained from the Kingston Lab (Massachusetts General Hospital-Harvard Medical School). An N-terminal FLAG-epitope tag was added to the JARID2 pFastBac1 vector. To assemble the full PRC2 complex, Sf9 cells were co-infected with baculovirus encoding FLAG-EZH2 and untagged SUZ12, EED, RbpA48. PRC2 subcomplexes were assembled *in vivo* by co-infecting Sf9 cells with the appropriate subset of these viruses and co-purified via the tagged subunit. When present, EZH2 was the FLAG-tagged subunit. In subcomplexes not containing EZH2, SUZ12 was tagged. JARID2 was the FLAG-tagged subunit in the PRC2-JARID2 co-purified complexes. Protein extract were prepared by three freeze-thaw cycles in lysis buffer (50 mM Tris-HCl pH 8.0, 300 mM NaCl, 1% NP-40, 0.3% Triton-X, 4 mM EDTA, 1 mM MgCl2, 1 mM DTT, 20% Glycerol and complete protease inhibitors (Roche)).

M2 anti-FLAG beads (Sigma) were used for all purifications. Proteins were bound to M2 beads in lysis buffer with 500 mM NaCl for 4h at 4°C. Beads were washed twice with 1000 mM NaCl in TAP buffer (50 mM Tris-HCl pH 7.9, 0.11% NP-40, 0.2 mM EDTA, 5 mM MgCl2, 2 mM DTT, 15% Glycerol and complete protease inhibitors (Roche)), twice with TAP-500mM NaCl and two more times with TAP-100 mM NaCl. Proteins were eluted with 1 hr incubations with 0.2 μg/ml 3X-FLAG peptide (Sigma). Eluates were concentrated using Amicon ultra 100 kDa MWCO concentrators (Millipore) to separate assembled complexes from free proteins. A 150 kDa Pierce® concentrator was used as a final step in the

purification of the PRC2:JARID2 complexes. Protein concentrations were determined by Bradford assay and purity was estimated from colloidal coomassie (Biorad) and silver stained protein gels. Nucleic acid contamination was evaluated by ^{32}P labeling of a phenol:chloroform treated sample.

FLAG-tag removal

FLAG-tagged PRC2 complex was incubated for with 1U rEnterokinase (Novagen®) in 1X reaction buffer with 0.025% Tween-20 for 1h at RT. A mock treatment of PRC2 was performed in the absence of enzyme under the same conditions. Reactions were stopped by the addition of NaCl to 300mM and 2mM DTT final concentrations. rEnterokinase was removed by ultrafiltration.

RNA Transcription and labeling

Templates containing the T7 promoter were generated by PCR with ExTaq DNA polymerase (Takara). PCR products were cloned and sequenced. AmpliScribe T7-Flash Transcription Kit (Epicentre) was used for transcription. After DNase treatment, samples were PAGE-purified in a 6% gel. RNA was eluted from gel slices by incubation for 1h at 30°C in elution buffer (10mM Tris-HCl pH 8.0, 500mM Sodium Acetate, 1mM EDTA and 0.1% SDS) and EtOH precipitated.

RNAs were dephosphorylated with Calf Intestinal Alkaline Phosphatase (NEB) and 5′-end labeled with T4 Polynucleotide Kinase (NEB) and [γ-^{32}P] ATP (Perkin Elmer). Labeled RNAs were gel purified, EtOH precipitated and quantified by liquid scintillation counting.

Electrophoretic Mobility Shift Assays

Labeled RNAs were pre-folded in buffer TE+300mM NaCl by incubating for 1 minute at 95°C, followed by a gradual decrease to room temperature. 10mM Tris-HCl pH 8.0 and $MgCl_2$ were added and the RNAs were transferred to ice for a minimum of 10 minutes.

Binding reactions were assembled with 1μl of 2000 cpm/μl (2nM final concentration) folded RNA and purified protein at the shown concentrations in Binding Buffer (50mM Tris-HCl pH 8.0, 100mM NaCl, 5mM $MgCl_2$, 10μg/ml BSA, 0.05% NP40, 1mM DTT, 20U RNaseOUT (Invitrogen) and 5% Glycerol) in 20μl. 50ng/μl yeast tRNA (Ambion® Cat# AM7119) was used as a nonspecific competitor and *E. coli*-expressed Glutathione *S*-transferase (GST) was used as negative control at the highest protein concentration in the particular experiment. After 20 min at 30°C the sample was loaded onto a 0.6% high-strength agarose (Sigma) gel in THEM buffer (66mM HEPES, 34mM Tris, 0.1mM disodium EDTA and 10mM $MgCl_2$) and run for 90 min at 90 volts at 4°C. Gels were dried and exposed to phosphorimager screens.

Double-Filter Binding Assays

Reactions were assembled as described above in a 30μl final volume. RNA titrations were performed with decreasing concentrations of prefolded RNA using a labeled RNA tracer. After 30 min at 30°C, the reactions were filtered through nitrocellulose (PROTRAN, Schleicher & Schuell) and Hybond-N+ (GE Healthcare) membranes using a Minifold I

system (Whatman), washed with 600µl Washing Buffer (50mM Tris-HCl pH 8.0, 100mM NaCl, 1.5mM $MgCl_2$, 0.05% NP40, 1mM DTT), dried, exposed to a phosphor screen and scanned after 2h in a Typhoon Trio (GE Healthcare Life Sciences). Data were quantified by Quantity One® and normalized as previously described (Wong and Lohman, 1993). Equilibrium dissociation constants, Kd, were obtained by non-linear regression of the binding data fitted to a one-site binding model using Graphpad Prism®.

HMTase Assays

5S Nucleosomal arrays were assembled with purified *E. coli* expressed core histones by gradient salt dialysis as described (Utley et al., 1998;Sif et al., 2001). HMTase reactions were assembled in Methylation Buffer (50mM Tris-HCl pH 8.5, 5mM $MgCl_2$ and 4mM DTT) containing nucleosomes, 0.33mM [^{3}H]-S-adenosyl-methionine (Perkin Elmer), the indicated [RNA] and PRC2 and incubated at 30°C. Fixed-time assays were incubated for 60 min, while for kinetic assays aliquots (15uL for reactions with 150nM PRC2, 30uL for reactions with 20nM PRC2) were removed at the indicated times and quenched with laemmli buffer, resolved by 18% SDS-PAGE, and transferred to an Immobilon-P membrane (Millipore). Blots were Coomassie stained, sprayed with EN^{3}HANCE (Perkin Elmer) and exposed to film. ^{3}H-methyl incorporation was measured by scintillation counting of excised histone H3 bands. Plotting the incorporation of ^{3}H-methyl groups as a function of time and obtaining the slope of the resulting straight line yielded the steady-state rates. IC_{50} values were determined by fitting the normalized rate data to a non-linear regression dose-response curve using Graphpad Prism® software.

Supplementary Material

Refer to Web version on PubMed Central for supplementary material.

Acknowledgments

We thank T. Cech and C. Davidovich for stimulating discussions and sharing results ahead of publication. We also thank members of the Lee lab for ongoing discussions; R. Kingston for critical reading and discussion; C.C. Richardson for support of A.J.H.; B. del Rosario for GST and FLAG-GFP proteins; R. Kingston and B. Ardehali for providing plasmids and baculovirus encoding the PRC2 subunits and JARID2; and L. Yang for graphics templates. This work is supported by grants from the National Institutes of Health (F32-GM101828-01 to C.C.-R; F32-GM101761-01 to A.J.H; and RO1-GM090278 to J.T.L.). J.T.L. is an investigator of the Howard Hughes Medical Institute.

References

Cao R, Zhang Y. SUZ12 is required for both the histone methyltransferase activity and the silencing function of the EED-EZH2 complex. Mol Cell. 2004; 15:57–67. [PubMed: 15225548]

Cloos PA, Christensen J, Agger K, Helin K. Erasing the methyl mark: histone demethylases at the center of cellular differentiation and disease. Genes Dev. 2008; 22:1115–1140. [PubMed: 18451103]

da Rocha ST, Boeva V, Escamilla-Del-Arenal M, Ancelin K, Granier C, Matias NR, Sanulli S, Chow J, Schulz E, Picard C, et al. JARID2 Is Implicated in the Initial Xist-Induced Targeting of PRC2 to the Inactive X Chromosome. Mol Cell. 2014; 53:301–316. [PubMed: 24462204]

Davidovich C, Zheng L, Goodrich KJ, Cech TR. Promiscuous RNA binding by Polycomb repressive complex 2. Nat Struct Mol Biol. 2013

Disteche CM. Dosage compensation of the sex chromosomes. Annu Rev Genet. 2012; 46:537–560. [PubMed: 22974302]

Duszczyk MM, Wutz A, Rybin V, Sattler M. The Xist RNA A-repeat comprises a novel AUCG tetraloop fold and a platform for multimerization. RNA. 2011; 17:1973–1982. [PubMed: 21947263]

Helin K, Dhanak D. Chromatin proteins and modifications as drug targets. Nature. 2013; 502:480–488. [PubMed: 24153301]

Jeon Y, Lee JT. YY1 Tethers Xist RNA to the Inactive X Nucleation Center. Cell. 2011; 146:119–133. [PubMed: 21729784]

Kaneko S, Bonasio R, Saldana-Meyer R, Yoshida T, Son J, Nishino K, Umezawa A, Reinberg D. Interactions between JARID2 and noncoding RNAs regulate PRC2 recruitment to chromatin. Mol Cell. 2014; 53:290–300. [PubMed: 24374312]

Kaneko S, Li G, Son J, Xu CF, Margueron R, Neubert TA, Reinberg D. Phosphorylation of the PRC2 component Ezh2 is cell cycle-regulated and up-regulates its binding to ncRNA. Genes Dev. 2010; 24:2615–2620. [PubMed: 21123648]

Kaneko S, Son J, Shen SS, Reinberg D, Bonasio R. PRC2 binds active promoters and contacts nascent RNAs in embryonic stem cells. Nature Structural and Molecular Biology. 2013 ePub 20 October 2013.

Kanhere A, Viiri K, Araujo CC, Rasaiyaah J, Bouwman RD, Whyte WA, Pereira CF, Brookes E, Walker K, Bell GW, et al. Short RNAs are transcribed from repressed polycomb target genes and interact with polycomb repressive complex-2. Molecular cell. 2010; 38:675–688. [PubMed: 20542000]

Khalil AM, Guttman M, Huarte M, Garber M, Raj A, Rivea Morales D, Thomas K, Presser A, Bernstein BE, van Oudenaarden A, et al. Many human large intergenic noncoding RNAs associate with chromatin-modifying complexes and affect gene expression. Proc Natl Acad Sci U S A. 2009

Kim W, Bird GH, Neff T, Guo G, Kerenyi MA, Walensky LD, Orkin SH. Targeted disruption of the EZH2-EED complex inhibits EZH2-dependent cancer. Nat Chem Biol. 2013; 9:643–650. [PubMed: 23974116]

Ku M, Koche RP, Rheinbay E, Mendenhall EM, Endoh M, Mikkelsen TS, Presser A, Nusbaum C, Xie X, Chi AS, et al. Genomewide analysis of PRC1 and PRC2 occupancy identifies two classes of bivalent domains. PLoS Genet. 2008; 4:e1000242. [PubMed: 18974828]

Lee JT. Epigenetic regulation by long noncoding RNAs. Science. 2012; 338:1435–1439. [PubMed: 23239728]

Lee JT, Davidow LS, Warshawsky D. Tsix, a gene antisense to Xist at the X-inactivation centre. Nat Genet. 1999; 21:400–404. [PubMed: 10192391]

Lee TI, Jenner RG, Boyer LA, Guenther MG, Levine SS, Kumar RM, Chevalier B, Johnstone SE, Cole MF, Isono K, et al. Control of developmental regulators by Polycomb in human embryonic stem cells. Cell. 2006; 125:301–313. [PubMed: 16630818]

Li G, Margueron R, Ku M, Chambon P, Bernstein BE, Reinberg D. JARID2 and PRC2, partners in regulating gene expression. Genes Dev. 2010; 24:368–380. [PubMed: 20123894]

Maenner S, Blaud M, Fouillen L, Savoye A, Marchand V, Dubois A, Sanglier-Cianferani S, Van Dorsselaer A, Clerc P, Avner P, et al. 2-D structure of the A region of Xist RNA and its implication for PRC2 association. PLoS Biol. 2010; 8:e1000276. [PubMed: 20052282]

Margueron R, Reinberg D. The Polycomb complex PRC2 and its mark in life. Nature. 2011; 469:343–349. [PubMed: 21248841]

Mercer TR, Mattick JS. Structure and function of long noncoding RNAs in epigenetic regulation. Nat Struct Mol Biol. 2013; 20:300–307. [PubMed: 23463315]

Minks J, Baldry SE, Yang C, Cotton AM, Brown CJ. XIST-induced silencing of flanking genes is achieved by additive action of repeat a monomers in human somatic cells. Epigenetics Chromatin. 2013; 6:23. [PubMed: 23915978]

Muller J, Verrijzer P. Biochemical mechanisms of gene regulation by polycomb group protein complexes. Curr Opin Genet Dev. 2009; 19:150–158. [PubMed: 19345089]

Nagano T, Fraser P. No-nonsense functions for long noncoding RNAs. Cell. 2011; 145:178–181. [PubMed: 21496640]

Ogawa Y, Sun BK, Lee JT. Intersection of the RNA Interference and X-Inactivation Pathways. Science. 2008; 320:1336–1341. [PubMed: 18535243]

Pandey RR, Mondal T, Mohammad F, Enroth S, Redrup L, Komorowski J, Nagano T, Mancini-Dinardo D, Kanduri C. Kcnq1ot1 antisense noncoding RNA mediates lineage-specific transcriptional silencing through chromatin-level regulation. Mol Cell. 2008; 32:232–246. [PubMed: 18951091]

Pasini D, Cloos PA, Walfridsson J, Olsson L, Bukowski JP, Johansen JV, Bak M, Tommerup N, Rappsilber J, Helin K. JARID2 regulates binding of the Polycomb repressive complex 2 to target genes in ES cells. Nature. 2010; 464:306–310. [PubMed: 20075857]

Peng JC, Valouev A, Swigut T, Zhang J, Zhao Y, Sidow A, Wysocka J. JARID2/Jumonji coordinates control of PRC2 enzymatic activity and target gene occupancy in pluripotent cells. Cell. 2009; 139:1290–1302. [PubMed: 20064375]

Qi W, Chan H, Teng L, Li L, Chuai S, Zhang R, Zeng J, Li M, Fan H, Lin Y, et al. Selective inhibition of Ezh2 by a small molecule inhibitor blocks tumor cells proliferation. Proc Natl Acad Sci U S A. 2012; 109:21360–21365. [PubMed: 23236167]

Ringrose L, Paro R. Epigenetic regulation of cellular memory by the Polycomb and Trithorax group proteins. Annu Rev Genet. 2004; 38:413–443. [PubMed: 15568982]

Rinn JL, Chang HY. Genome regulation by long noncoding RNAs. Annu Rev Biochem. 2012; 81:145–166. [PubMed: 22663078]

Rinn JL, Kertesz M, Wang JK, Squazzo SL, Xu X, Brugmann SA, Goodnough LH, Helms JA, Farnham PJ, Segal E, et al. Functional demarcation of active and silent chromatin domains in human HOX loci by noncoding RNAs. Cell. 2007; 129:1311–1323. [PubMed: 17604720]

Schuettengruber B, Cavalli G. Recruitment of polycomb group complexes and their role in the dynamic regulation of cell fate choice. Development. 2009; 136:3531–3542. [PubMed: 19820181]

Schwartz YB, Pirrotta V. Polycomb complexes and epigenetic states. Curr Opin Cell Biol. 2008; 20:266–273. [PubMed: 18439810]

Shen X, Kim W, Fujiwara Y, Simon MD, Liu Y, Mysliwiec MR, Yuan GC, Lee Y, Orkin SH. Jumonji modulates polycomb activity and self-renewal versus differentiation of stem cells. Cell. 2009; 139:1303–1314. [PubMed: 20064376]

Sif S, Saurin AJ, Imbalzano AN, Kingston RE. Purification and characterization of mSin3A-containing Brg1 and hBrm chromatin remodeling complexes. Genes Dev. 2001; 15:603–618. [PubMed: 11238380]

Simon JA, Kingston RE. Occupying chromatin: Polycomb mechanisms for getting to genomic targets, stopping transcriptional traffic, and staying put. Mol Cell. 2013; 49:808–824. [PubMed: 23473600]

Sing A, Pannell D, Karaiskakis A, Sturgeon K, Djabali M, Ellis J, Lipshitz HD, Cordes SP. A vertebrate Polycomb response element governs segmentation of the posterior hindbrain. Cell. 2009; 138:885–897. [PubMed: 19737517]

Son J, Shen SS, Margueron R, Reinberg D. Nucleosome-binding activities within JARID2 and EZH1 regulate the function of PRC2 on chromatin. Genes Dev. 2013; 27:2663–2677. [PubMed: 24352422]

Starmer J, Magnuson T. A new model for random X chromosome inactivation. Development. 2009; 136:1–10. [PubMed: 19036804]

Tsai MC, Manor O, Wan Y, Mosammaparast N, Wang JK, Lan F, Shi Y, Segal E, Chang HY. Long noncoding RNA as modular scaffold of histone modification complexes. Science. 2010; 329:689–693. [PubMed: 20616235]

Utley RT, Ikeda K, Grant PA, Cote J, Steger DJ, Eberharter A, John S, Workman JL. Transcriptional activators direct histone acetyltransferase complexes to nucleosomes. Nature. 1998; 394:498–502. [PubMed: 9697775]

Wong I, Lohman TM. A double-filter method for nitrocellulose-filter binding: application to protein-nucleic acid interactions. Proc Natl Acad Sci U S A. 1993; 90:5428–5432. [PubMed: 8516284]

Woo CJ, Kharchenko PV, Daheron L, Park PJ, Kingston RE. A region of the human HOXD cluster that confers polycomb-group responsiveness. Cell. 2010; 140:99–110. [PubMed: 20085705]

Wu L, Murat P, Matak-Vinkovic D, Murrell A, Balasubramanian S. Binding interactions between long noncoding RNA HOTAIR and PRC2 proteins. Biochemistry. 2013; 52:9519–9527. [PubMed: 24320048]

Wutz A. Gene silencing in X-chromosome inactivation: advances in understanding facultative heterochromatin formation. Nat Rev Genet. 2011; 12:542–553. [PubMed: 21765457]

Wutz A, Gribnau J. X inactivation Xplained. Curr Opin Genet Dev. 2007; 17:387–393. [PubMed: 17869504]

Wutz A, Rasmussen TP, Jaenisch R. Chromosomal silencing and localization are mediated by different domains of Xist RNA. Nat Genet. 2002; 30:167–174. [PubMed: 11780141]

Yap KL, Li S, Munoz-Cabello AM, Raguz S, Zeng L, Mujtaba S, Gil J, Walsh MJ, Zhou MM. Molecular interplay of the noncoding RNA ANRIL and methylated histone H3 lysine 27 by polycomb CBX7 in transcriptional silencing of INK4a. Mol Cell. 2010; 38:662–674. [PubMed: 20541999]

Yuan W, Wu T, Fu H, Dai C, Wu H, Liu N, Li X, Xu M, Zhang Z, Niu T, et al. Dense chromatin activates Polycomb repressive complex 2 to regulate H3 lysine 27 methylation. Science. 2012; 337:971–975. [PubMed: 22923582]

Zhao J, Ohsumi TK, Kung JT, Ogawa Y, Grau DJ, Sarma K, Song JJ, Kingston RE, Borowsky M, Lee JT. Genome-wide identification of polycomb-associated RNAs by RIP-seq. Mol Cell. 2010; 40:939–953. [PubMed: 21172659]

Zhao J, Sun BK, Erwin JA, Song JJ, Lee JT. Polycomb proteins targeted by a short repeat RNA to the mouse X chromosome. Science. 2008; 322:750–756. [PubMed: 18974356]

HIGHLIGHTS

- PRC2 binds RNA selectively with high specificity.
- EZH2 is somewhat promiscuous and EED lends specificity to PRC2-RNA interactions.
- RNA inhibits PRC2's histone methyltransferase activity.
- JARID2 attenuates RNA binding and relieves inhibition of methylation.

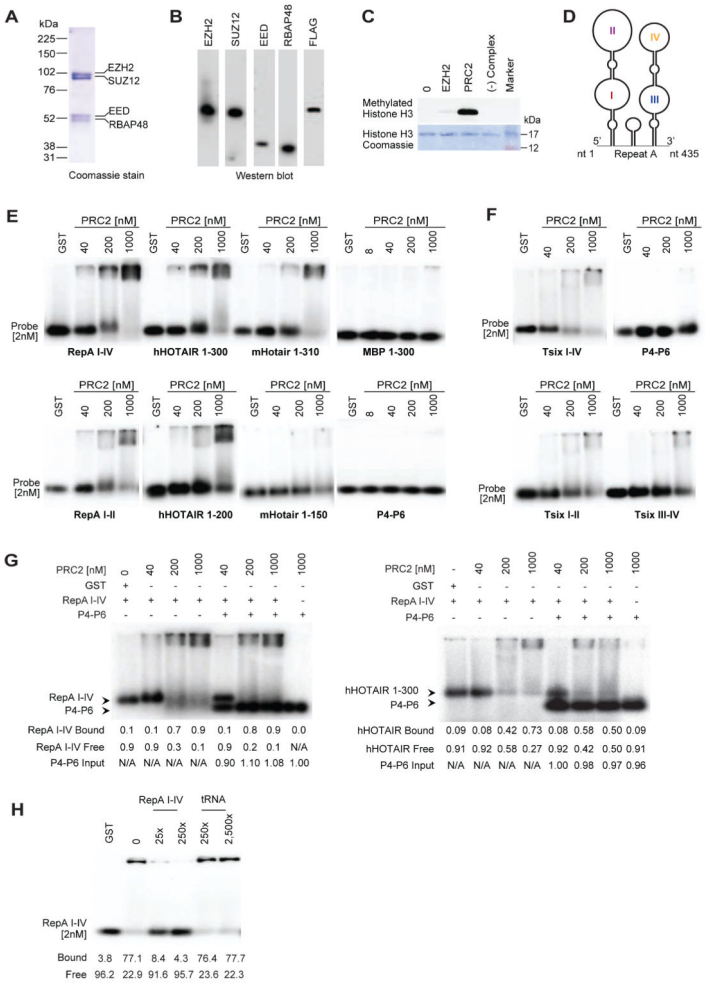

Figure 1. PRC2 discriminates between cognate and nonspecific RNA

(**A,B**) Coomassie staining (**A**) and Western blotting (**B**) of purified mouse PRC2 subunits. (**C**) HMTase assay (top) and Coomassie staining of H3 (bottom) show that purified PRC2 is active. (**D**) RepA stem-loop structures I-IV (Maenner et al., 2010). (**E,F**) EMSAs with long (≥300nt) (**E**) and shorter (≤200nt) (**F**) RNA probes. Tsix I-IV, antisense of RepA I-IV. Tsix I-II, antisense of RepA I-II. Tsix III-IV, antisense of RepA II-IV. Probe used at 2nM unless otherwise indicated. PRC2 concentrations between 40–1000nM as shown. GST, 1000nM. (**G**) Two-probe competition experiments. Left: Competition between RepA I-IV and P4-P6 shows PRC2's specific preference for RepA I-IV over P4-P6. RNA and PRC2 concentrations as indicated in nM. Quantification of RepA I-IV bound and free fractions, as well as P4-P6 input are indicated. Right: Competition between hHOTAIR 1-300 and P4-P6 for the same PRC2 pool shows preference for hHOTAIR 1-300 over P4-P6 further showing PRC2 specific RNA recognition capability. Quantification of hHOTAIR 1-300 bound and free fractions, as well as P4-P6 input are indicated. (**H**) EMSA with 2nM RepA I-IV probe and cold competitor (RepA I-IV, tRNA) at indicated concentrations. Please also refer to Figures S1 and S2.

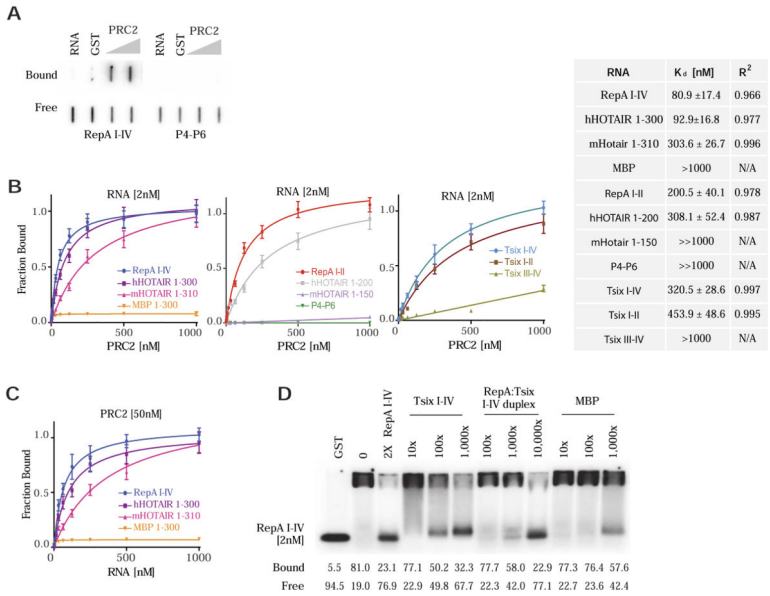

RNA	K_d [nM]	R^2
RepA I-IV	80.9 ±17.4	0.966
hHOTAIR 1-300	92.9±16.8	0.977
mHotair 1-310	303.6 ± 26.7	0.996
MBP	>1000	N/A
RepA I-II	200.5 ± 40.1	0.978
hHOTAIR 1-200	308.1 ± 52.4	0.987
mHotair 1-150	>>1000	N/A
P4-P6	>>1000	N/A
Tsix I-IV	320.5 ± 28.6	0.997
Tsix I-II	453.9 ± 48.6	0.995
Tsix III-IV	>1000	N/A

Figure 2. A range of PRC2-RNA binding affinities

(**A**) Example of double-filter binding assay used to obtain binding isotherms and K_d values. Top (bound), nitrocellulose membrane. Bottom (free), Hybond-N+ membrane. (**B**) Binding isotherms of PRC2 to 2 nM RNA of species indicated. Equilibrium dissociation constants (K_d) and R^2 values shown in table. N/A, not applicable because curves were too flat. "≫1000 nM" denotes a K_d in excess of that which could be measured under our assay conditions. (**C**) Reciprocal binding experiments in which 1–1000nM RNA is titrated against constant 50nM PRC2, with K_d and R^2 values shown. A labeled corresponding RNA (<1%) was used as tracer. (**D**) EMSA using 2nM RepA I-IV probe in the presence of cold competitor RNA species (RepA I-IV, Tsix I-IV, RepA I-IV: Tsix I-IV pre-annealed duplex, MBP) at indicated concentrations.

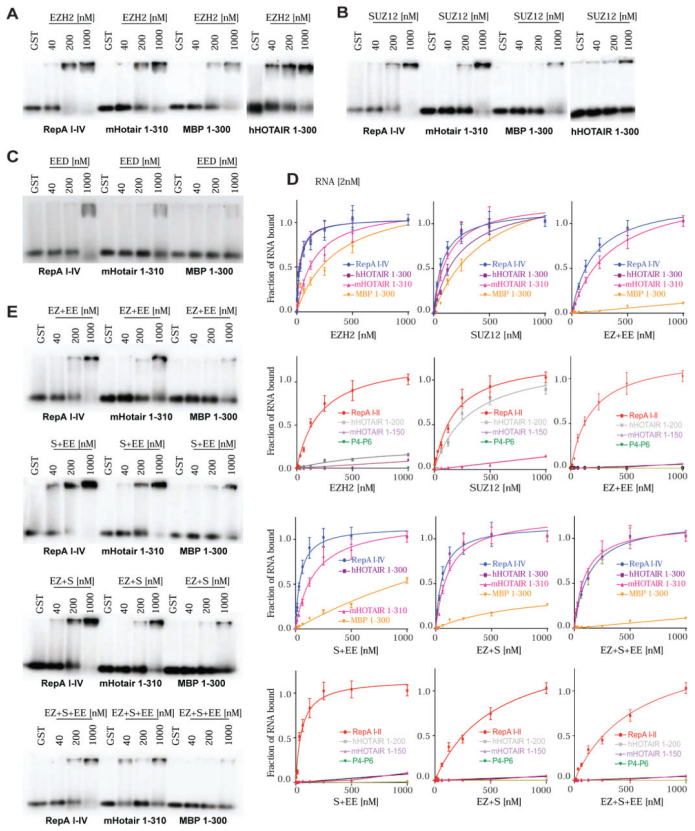

F

RNA	EZH2 Kd [nM]	EZH2 R^2	SUZ12 Kd [nM]	SUZ12 R^2	EZH2+EED Kd [nM]	EZH2+EED R^2	SUZ12+EED Kd [nM]	SUZ12+EED R^2	EZH+SUZ12 Kd [nM]	EZH+SUZ12 R^2	EZH2+SUZ12+EED Kd [nM]	EZH2+SUZ12+EED R^2
RepA I-IV	31.8±4.2	0.965	86.48 ±13.7	0.9622	199.9±24.6	0.992	44.75 ±4.8	0.991	62.6±7.4	0.991	138.7 ±15.9	0.962
hHOTAIR 1-300	28.4±3.4	0.968	235.5±30.7	0.9932	ND	ND	ND	ND	ND	ND	ND	ND
mHotair 1-310	157.2± 26.7	0.996	132.2 ± 26.7	0.9642	371.4±11.3	0.996	169 ± 18.7	0.993	119.8± 29.4	0.968	97.5 ± 9.7	0.964
MBP	379.5±122.3	0.914	501.9±125.8	0.9802	>1000	N/A	>1000	N/A	893.2±272.2	0.950	>1000	0.993
RepA I-II	216.5±32.7	0.966	202.4 ±34.2	0.9867	280.7±43.4	0.989	54.1 ±9.6	0.979	566.8.5±103.7	0.921	582.2 ±85.8	0.983
hHOTAIR 1-200	911.2±389.3	0.961	327.0±74.6	0.9795	ND	ND	ND	ND	ND	ND	ND	ND
mHotair 1-150	>1000	N/A	>1000	N/A	>1000	N/A	>1000	N/A	>1000	N/A	>1000	N/A
P4-P6	> 1000	N/A	>1000	N/A	> 1000	N/A	>1000	N/A	> 1000	N/A	>1000	N/A

Figure 3. RNA binding potential of PRC2 subunits and subcomplexes

(**A**) EMSA shows high affinity of EZH2 (concentrations shown) for RNA. (**B**) EMSA shows that SUZ12 also binds RNA but at higher concentrations. (**C**) EMSA shows that EED binds poorly to all tested RNAs. (**D**) Binding isotherms of PRC2 single subunits EZH2 and SUZ12, and subcomplexes: EZH2+EED (EZ+EE), SUZ12+EED (S+EE), EZH2+SUZ12 (EZ+S) and EZH2+SUZ12+EED (EZ+S+EE). Isotherms generated from data obtained from double-filter binding experiments. (**E**) EMSAs showing PRC2 subcomplexes interactions with long (≥300nt) RNAs. (First panel) shows that EED (EE) attenuates EZH2 (EZ) binding to RNA. (Second panel) EMSA shows that EED has modest effects on SUZ12 binding to RNA. (Third panel) EMSA shows that the EZH2-SUZ12 subcomplex (EZ+S) also binds RNA, but with lower affinity that EZH2 alone. (Bottom) EMSA of the EZH2-SUZ12-EED subcomplex (EZ+S+EE) showing reduced RNA binding. (**F**) Table of K_d and R^2 values for PRC2 single subunits- and PRC2 subcomplexes-RNA interactions. Please also refer to Figure S2.

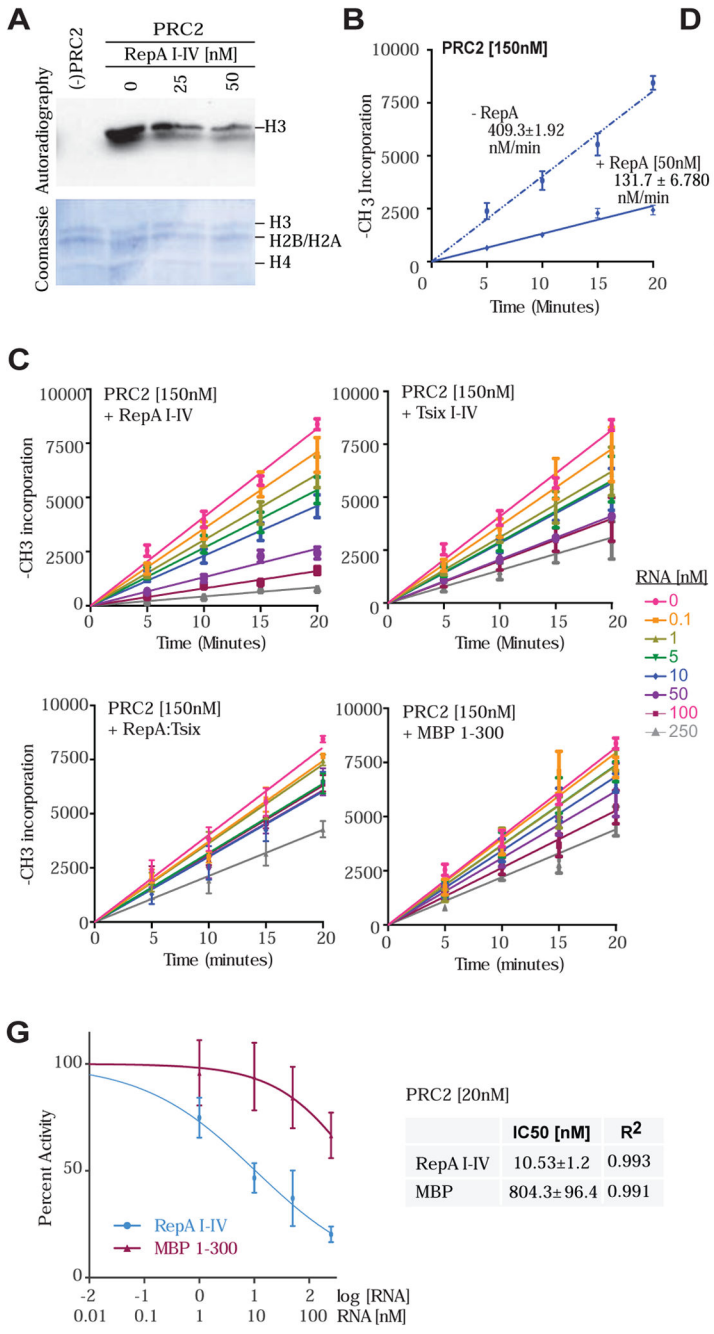

D

No RNA	409.3 ± 11.92			
RNA [nM]	**RepA I-IV**	**Tsix I-IV**	**RepA:Tsix**	**MBP**
0.1	355.8 ± 5.9	363.8 ± 14.3	371.6 ± 9.7	397.3 ± 16.3
1	303.2 ± 6.2	310.5 ± 11.7	363.7 ± 8.0	367.5 ± 10.8
5	267.3 ± 5.3	288.6 ± 10.8	319.1 ± 6.5	368.9 ± 10.7
10	230.8 ± 3.8	282.9 ± 11.7	301.3 ±1 1.0	342.6 ± 9.9
50	131.7 ± 6.8	205.5 ± 1.4	303.9 ±10.0	308.7 ±1 1.0
100	80.22 ± 3.4	199.0 ± 10.3	314.8 ± 8.5	264.0 ± 8.8
250	42.90 ± 2.7	154.6 ± 9.7	212.9 ± 8.7	220.5 ± 10.0

E

PRC2 [150nM]

	IC50 [nM]	R^2
RepA I-IV	9.7±3.5	0.974
Tsix I-IV	47.9±11.3	0.986
RepA:Tsix	>1000	N/A
MBP	981.8± 502.2	0.988

F

RNA	P
RepA I-IV vs Tsix I-IV	0.0053
RepA I-IV vs MBP	0.0048
Tsix I-IV vs MBP	0.0055
RepA I-IV vs RepA:Tsix	0.0076
Tsix I-IV vs RepA:Tsix	0.0150
MBP vs RepA:Tsix	0.5430

G

PRC2 [20nM]

	IC50 [nM]	R^2
RepA I-IV	10.53±1.2	0.993
MBP	804.3± 96.4	0.991

Figure 4. RNA suppresses the histone methyltransferase activity of EZH2

(**A**) Effect of RepA I-IV on the activity of purified PRC2. HMTase assay (top) and Coomassie staining (bottom) of *in vitro*-assembled recombinant nucleosomes (bottom) showing active PRC2. PRC2 (150nM). RepA concentrations are indicated. (**B**) Kinetics of histone H3 methylation by PRC2 showing an inhibitory effect of 50nM RepA I-IV. The incorporation of ^{3}H-methyl groups into histone H3 is plotted as a function of time. (**C**) Kinetics of histone H3 methylation by PRC2 showing changes in inhibition at increasing concentrations of various RNA species. Legend indicates [RNA] in nM. (**D**) Table depicting

the steady-state rates of histone H3 methylation by PRC2 in the presence of different RNAs from (C). (**E**) Histone H3 methylation rate as a function of RNA concentration at 150nM PRC2. The plot shows the percentage of the methylation rate exhibited at a given [RNA] compared to the rate in the absence of RNA (100%). The RNA concentration is plotted on a log scale, with the corresponding linear values indicated on the bottom. Corresponding table shows the IC_{50} and R^2 values for tested RNAs. (**F**) Comparison of the data in (**E**) among RNA species shows that the dose-response behavior of the methylation rate in response to different RNAs exhibits significant differences. (**G**) Plot showing percent of Histone H3 methylation activity as a function of RNA concentration at 20nM PRC2. Table shows the IC_{50} and R^2 values for RepA I-IV and MBP 1-300. (**B–G**) Data are presented as mean ± SD.

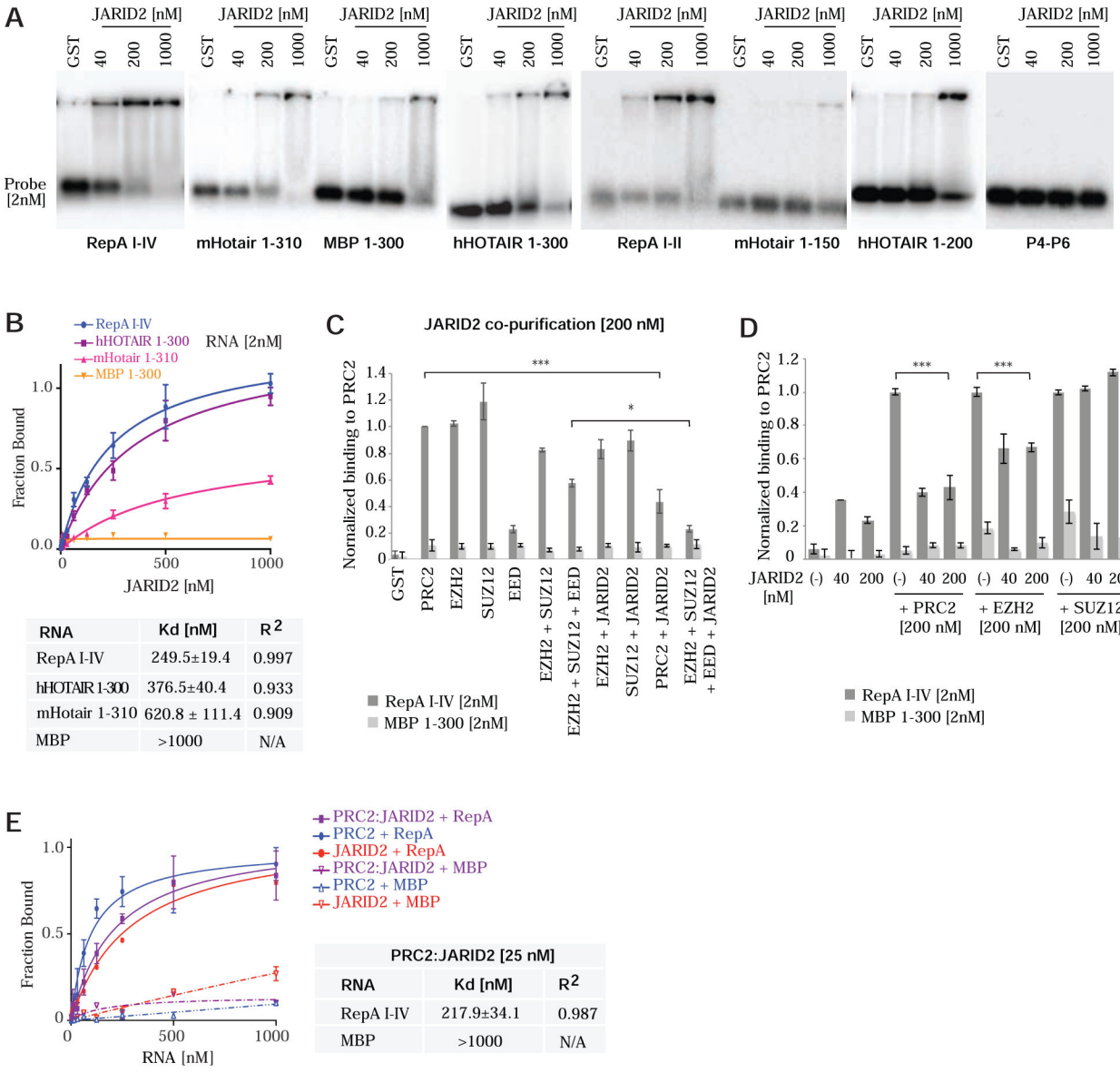

Figure 5. JARID2 binds RNA with modest affinity but strongly attenuates PRC2 binding to RNA

(**A**) EMSA shows that JARID2 binds specifically but with moderate affinity to different size RNAs. (**B**) Binding isotherms of JARID2 to indicated RNAs. Equilibrium dissociation constants (K_d) and R^2 values shown in table. (**C**) Average of three double-filter binding experiments showing a significant decrease on RNA binding in PRC2 complexes containing EED and JARID2. Data normalized to PRC2 binding. Minimal protein binding to MBP is observed at 200nM protein. (**D**) Significant decrease on RNA binding to PRC2 and EZH2 is also observed when purified JARID2 is added to PRC2 complexes in double-filter binding experiments. RNA[2nM] and protein concentrations are indicated. Data normalized to PRC2 binding. (**E**) Binding isotherms for 25nM protein complexes that include PRC2 and/or JARID2. In PRC2:JARID2 reactions, JARID2 was added stoichiometrically to PRC2. RNAs of indicated species are titrated. K_d and R^2 values shown in table. (**B–G**) Data are presented

as mean ± SD. Please also see Figure S3 for the reciprocal titrations, which yielded similar results.

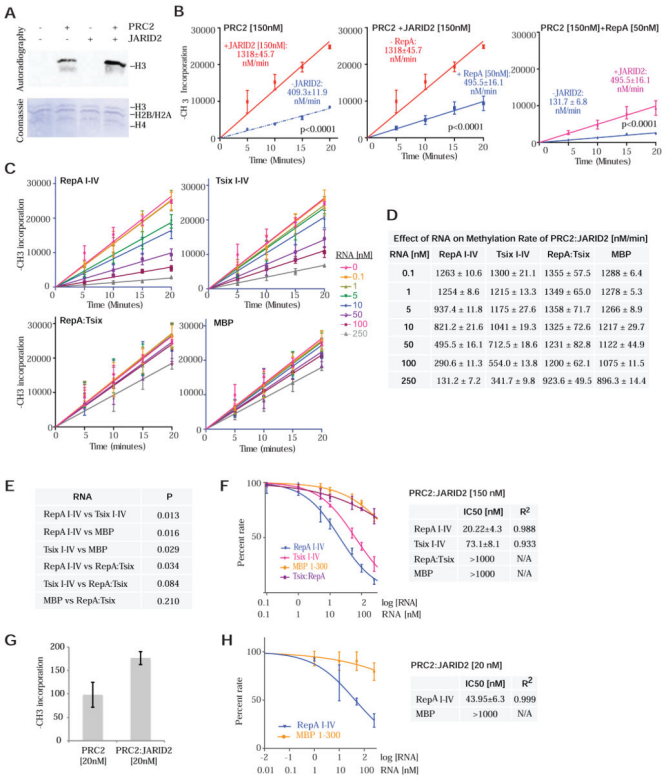

Figure 6. Regulatory interactions of PRC2, JARID2, and RNA at the chromatin interface

(**A**) Effect of JARID2 on the H3 methylation activity of purified PRC2. HMTase assay (top) and Coomassie staining (bottom) of in vitro assembled recombinant nucleosomes. Histones are indicated. JARID2 (150nM) and PRC2 (150nM). (**B**) Kinetics of histone H3 methylation by PRC2. Incorporation of ^{3}H-methyl groups into histone H3 is plotted as a function of time. (Left) Time-course of PRC2 histone H3 methylation showing increased methylation rate in the presence of 150nM JARID2. (Middle) Inhibitory effect of 50nM RepA I-IV. (Right) Addition of JARID2 (150nM) reduces the inhibitory effect of RepA on the rate of histone H3 methylation by PRC2 (150nM). The incorporation of ^{3}H-methyl groups into histone H3 is plotted as a function of time. (**C**) Kinetics of histone H3 methylation by PRC2 in the presence of JARID2 and increasing concentrations of various RNA species. (**D**) Table depicting the steady-state methylation rates in the presence of JARID2 (150nM) from (D). (**E**) Histone H3 methylation rate as a function of RNA concentration in the presence of JARID2. The plot shows the percentage of the methylation rate exhibited at a given [RNA] compared to the rate in the absence of RNA (100%). The RNA concentration is plotted on a log scale, with the corresponding values indicated on the bottom. The attached table shows the IC_{50} and R^2 values for the tested RNAs. (**F**) Comparison of the data in (E) among RNA species shows that the dose-response behavior of the methylation rate in response to different RNA exhibits significant differences. (**G**) Effect of JARID2 on the incorporation of ^{3}H-methyl groups into Histone H3 at 20nM PRC2. (**H**) Plot showing percent of Histone H3 methylation activity as a function of RNA concentration in the presence of 20nM PRC2 and JARID2. The RNA concentration is plotted on a log scale, with the corresponding linear

values indicated on the bottom. Corresponding table shows the IC_{50} and R^2 values for RepA I-IV and MBP 1-300. (**B**–**H**) Data are presented as mean ± SD.

Figure 7. Summary, synthesis, and model

(**A**) Summary and synthesis of our data in the context of published works, taking into account the cumulative *in vivo* and *in vitro* observations. (**B**) Proposed steps of PRC2 recruitment, chromatin loading, and H3K27 trimethylation, using RepA as a model. [1] High level expression of Tsix RNA titrates the RepA-PRC2 interaction, either by directly binding PRC2 or RepA (Ogawa et al., 2008; Zhao et al., 2008). Duplex RNA is inert for PRC2 binding (Fig. 1). [2] When Tsix is developmentally downregulated, RepA co-transcriptionally recruits PRC2 (Zhao et al., 2008). EZH2 binds RNA strongly; SUZ12 binds more weakly (Fig. 3). [3] After Tsix RNA is depleted, PRC2 loads onto chromatin, but its HMTase activity is held in check by RepA (Fig. 4). In the absence of JARID2 [4A], PRC2's HMTase activity is limited, but low-level H3K27me3 may be detected. [5A] PRC2 dissociates from chromatin without JARID2 on ChrX (da Rocha et al., 2014). When JARID2 is present [4B], RNA-EZH2 interactions are weakened and EZH2's HMTase activity is promoted, resulting in high levels of H3K27me3. JARID2 can act substoichiometrically but it is not known whether JARID2 is free or bound to chromatin. [5B] The PRC2:JARID2 complex efficiently spreads H3K27me3 along ChrX. (**C**) Schematic representation of positive and negative regulatory relationships among PRC2 subunits, JARID2, RNA, and the chromatin target. Green arrows, positive regulation. Red

arrows, negative regulation. Note that JARID2's relationship to PRC2's HMTase activity is "positive" via two sequential negative events.